Flux-dependent percolation transition in immiscible two-phase flows in porous media

Thomas Ramstad*
Department of Physics, Norwegian University of Science and Technology, N-7491 Trondheim, Norway and Numerical Rocks AS, Stiklestadveien 1, N-7041 Trondheim, Norway

Alex Hansen†
Department of Physics, Norwegian University of Science and Technology, N-7491 Trondheim, Norway

Pål-Eric Øren‡
Numerical Rocks AS, Stiklestadveien 1, N-7041 Trondheim, Norway

(Received 14 November 2008; published 20 March 2009)

Using numerical simulations, we study immiscible two-phase flow in a pore network reconstructed from Berea sandstone under flow conditions that are statistically invariant under translation. Under such conditions, the flow is a state function which is not dependent on initial conditions. We find a second-order phase transition resembling the phase inversion transition found in emulsions. The flow regimes under consideration are those of low surface tension—hence high capillary numbers Ca—where viscous forces dominate. Nevertheless, capillary forces are imminent, we observe a critical stage in saturation where the transition takes place. We determine polydispersity critical exponent $\tau = 2.27 \pm 0.08$ and find that the critical saturation depends on how fast the fluids flow.

DOI: 10.1103/PhysRevE.79.036310 PACS number(s): 47.56.+r, 05.65.+b, 47.55.dm, 47.55.nb

I. INTRODUCTION

There are several similarities between emulsions and two-phase flow of immiscible fluids in porous media. The two fluids, e.g., oil and water, would by themselves demix. However, in the porous medium the capillary forces, caused by the interactions between the solid matrix and the fluid interfaces, stabilize the fluid phases. In some sense the solid matrix acts as a "frozen" emulsifier. This leads to large differences between the two types of systems, since in one case the emulsifier follows the motion of the two fluids, whereas in the other case, the "emulsifier" is static. In emulsions, Bancroft's rule of thumb states that the more soluble phase constitutes the continuous phase [1]. This rule may be broken, but at least one of the fluids must form a continuous phase. In porous media on the other hand it is the solid matrix—the "static emulsifier"—that forms the continuous phase, whereas neither of the fluids needs to form a continuous phase.

Typically, experiments on two-phase flow in porous media are performed through flooding of an already saturated sample by another fluid [2]. Under such boundary conditions, the analogy with emulsions is not strong. However, as we shall see, under conditions where the two phases form structures that statistically have the same translational symmetries as the porous matrix, the analogy makes sense. We will in the following assume that the porous matrix is statistically invariant under translation.

We will in this paper study numerically the two-phase flow under such conditions using the reconstructed pore space of a Berea sandstone. As we will show, there is a phase transition resembling the phase inversion transition occurring in emulsions. This transition is driven by the interplay between pore-scale capillary forces and long-range viscous forces, and it concerns the distribution of clusters (bubbles) of the nonwetting fluid. We shall furthermore see that the transition, which is second order in character, depends not only on parameters such as the saturation but also on the flow rate. This is caused by the relative strength of the viscous forces to the capillary forces changing with the flow rate.

There have been studies of steady-state two-phase flow in the past, e.g., the "Penn State" method for measuring relative permeability requires steady-state conditions [3]. Avraam *et al.* [4] studied the dynamics of clusters in two-dimensional model porous media under simultaneous injection and flow of two immiscible fluids. This work has been followed up by a numerical work by Constantinides and Payatakes [5]. Hashemi *et al.* [6,7] generalized the invasion percolation algorithm to study steady-state flow numerically in the limit of capillary dominance.

II. STEADY-STATE MODEL

Steady-state conditions are defined in the literature as those characterized by statistical stationarity with respect to time. This definition is not equivalent to a state which is statistically invariant under spatial translation. Such a state is achievable in experiments involving simultaneous injection, but as the system is open, important flow parameters such as saturation are difficult to control [8]. We will in the following refer to the statistically translational invariant state as the *steady state*.

*thomas@numericalrocks.com
†alex.hansen@ntnu.no
‡peoe@numericalrocks.com

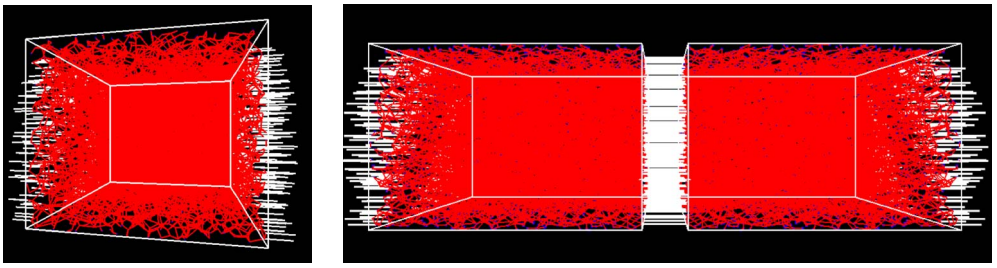

FIG. 1. (Color online) The network reconstructed from a Berea sandstone sample. The upper figure shows the original network [gray (red online)] with the inlet and outlet links colored white. In the lower figure the network is mirrored around the plane normal to the pressure gradient. This makes it possible to implement periodic boundary conditions in the flow direction.

Using a numerical model which has been thoroughly tested against experimental model porous media in two dimensions [9], we create such steady-state flow as described above, where we have full control over all flow parameters. An important observation is that the steady state at higher capillary numbers is independent of the initial conditions, i.e., it retains no memory of how it was started. It is a true *state* in the sense used in thermodynamics. Hence, the phase transition we study resembles closely those seen in equilibrium statistical mechanics.

We show in Fig. 1 the reconstructed network. It contains 12 349 nodes and 26 146 links including 521 links that make up the inlet and outlet of the original network. The sample from which it is reconstructed measured $(3\times3\times3\ \mathrm{mm}^3)$, with a total area of the inlet links of $0.225\ \mathrm{mm}^2$. More details on network reconstruction procedures may be found in the work of Øren *et al.* [10].

In order to create steady-state flow in this system, we need to impose periodic boundary conditions in the flow direction. This enables the configurations that leave the network at one side to enter the network at the opposite side. It is not possible to do this as the edges of the network do not match each other. We solve this problem by making a mirror copy of the network and connecting this copy in series with the original network, see Fig. 1. The edges then match and periodic boundary conditions in the flow direction may now be implemented.

Each bond in the network is characterized by the number of parameters that reflect the original pore in the original sandstone. The pores are triangular in shape, and each pore consists of two parts that make up the pore body and one part that connects them which resembles the pore throat. Each part is described by a shape factor G defined as the effective area of the pore divided by the square of its circumference. We assume that the wetting properties of the two fluids are such that the film flow does not occur, and the flow in the pores is assumed to be pistonlike. The mobility g_{ij} of a bond between nodes i and j is calculated from an average of the mobilities coming from the bodies and the throat. The single terms are given by

$$g = (3r^2A)/(20\mu_{\mathrm{eff}}), \tag{1}$$

where r is the inscribed radius of the pore defined by $A=r^2/(4G)$, which is the effective cross-sectional area. The effective viscosity μ_{eff} is the weighted average of the viscosities of the two fluids for each bond.

If p_i and p_j are the pressures at nodes i and j, respectively, so that $\Delta p_{ij}=p_i-p_j$, the flux between them is given by

$$q_{ij} = \frac{g_{ij}}{\ell_{ij}}(\Delta p_{ij} - p_c), \tag{2}$$

where p_c is the capillary pressure and ℓ_{ij} is the length between the center of the two pore bodies making up the nodes.

The capillary pressure p_c, which acts as a barrier for the nonwetting fluid to penetrate a pore body filled with wetting fluid, is calculated using the contact angle θ between the wetting and the nonwetting phases as $p_c=(2\gamma/r)\cos\theta$. In a more realistic case the contact angle is different in drainage and imbibition. The bonds are assumed to be hour glass shaped so that the dependence of the capillary pressure with respect to the position of the meniscus, x in the pore, is

$$p_c = \frac{2\gamma}{r_\ell}\left[1 - \cos\left(\frac{2\pi x}{\ell}\right)\right]. \tag{3}$$

The radius r_ℓ denote the throat radius which is the narrowest part of the pore space.

The flow equations are solved as a large set of linear equation, ensuring that the net flux in a node is zero according to mass conservation of immiscible fluids, $\Sigma_j q_{ij}=0$. We assume pistonlike creep flow in the links, and the volumes of both pore bodies and throats are associated with these links, leaving the nodes volumeless. A forward Euler integration scheme is implemented for tracking the motion of the interfaces. We use, however, an adaptive time step Δt so that the displacement of any given meniscus does not exceed a tenth of ℓ.

There are three dimensionless parameters that characterizes the two-phase flow: (1) the viscosity ratio $M=\mu_{\mathrm{nw}}/\mu_w$ between the nonwetting and wetting fluids, (2) the saturation, S_{nw}, which is the fraction of fluid in the porous medium that

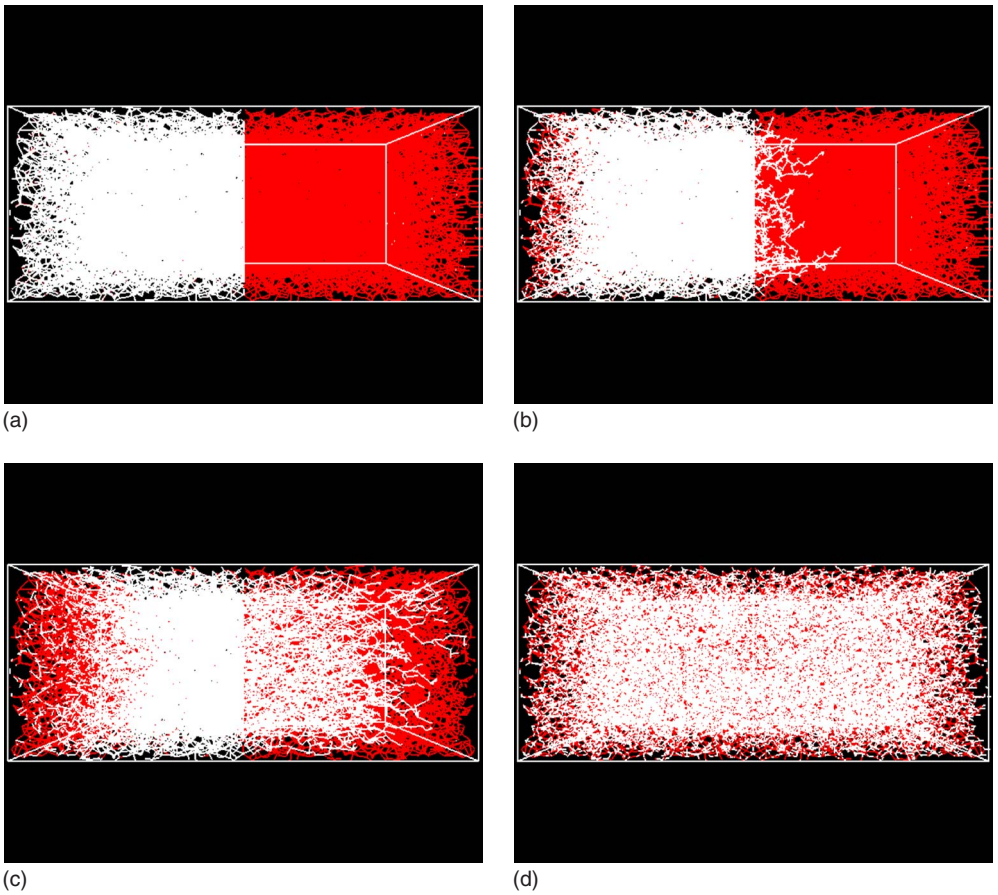

FIG. 2. (Color online) The evolution toward steady-state flow when the flux is $Q_{\mathrm{tot}}=1.0\times10^{-2}$ mm^3/s giving Ca$=3.0\times10^{-3}$. The system is initially divided into two distinct regions with one nonwetting phase (white) and one wetting phase [gray (red online)]. The three following snapshots show the system at $t\approx30$ s, $t\approx90$ s, and when the flow has reached steady state. The reader should note the fingering front where the nonwetting fluid enters the wetting fluid and the stable displacement front where the wetting fluid enters the nonwetting fluid in the two upper panels [11].

is nonwetting, and (3) the capillary number Ca, given by the ratio of the viscous to the capillary forces on the pore level,

$$\mathrm{Ca}=\frac{\mu_{\mathrm{eff}}Q}{\gamma\Sigma}, \tag{4}$$

where Σ is the area of the cross section of the porous medium and Q is the global flow rate. We assume the phases to be equal in density so that buoyancy effects may be neglected.

We set the surface tension to a low value $\gamma=0.03$ mN/m and viscosity for the wetting and nonwetting fluids to $\mu_{\mathrm{nw}}=\mu_w=0.1$ Pa s so that $M=\mu_{\mathrm{nw}}/\mu_w=1$. In order to control Ca we change the global flow rate Q_{tot}. The capillary numbers were varied from $\mathrm{Ca}\simeq1.0\times10^{-4}$ to $\mathrm{Ca}\simeq1.0$, corresponding to superficial fluid velocities ranging from $v_s\simeq1$ mm/h to $v_s\simeq1$ mm/s. Given the values of Ca, we are definitely in a flow regime dominated by viscous forces. However, the fluid phases remain immiscible and a steady-state configuration of the structures and macroscopic parameters is obtainable. We also note that since the system is closed, the saturation is set initially and does not change as the flow proceeds. The configuration shown in Fig. 2 was run on a single dual core processor with 2.4 GHz.

III. RESULTS

Our supreme hypothesis is that the steady-state fluid configurations do not depend on how the system started out but rather on the statistically invariant physical parameters acting on the system. It is nevertheless very interesting to observe and quantify how our system evolves into a steady-state behavior with transients which subsequently vanish.

Shown in Fig. 2 is a starting configuration of totally separated halves of hence wetting and nonwetting fluids. As a global pressure gradient $\Delta P/L$ is applied over the network of length L, the phases start to mobilize and create two distinct fronts, one of imbibition and one of drainage. This leads to forming of local meniscii between the different phases, and resistance caused by capillary forces will alter the transport. In order to keep a constant flow rate independent of the increased resistance, the global pressure drop ΔP will as a consequence increase.

This effect is shown in Fig. 3 and is clearly observable even though the flow regimes considered in this paper is in the viscous regime. A seemingly linear rise in ΔP is governed by the increasing number of fingers and meniscii in the network which at steady state will saturate around a mean

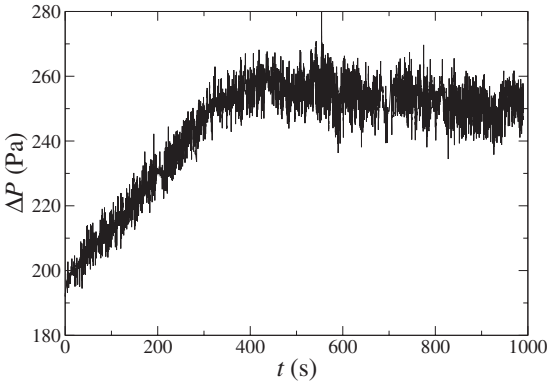

FIG. 3. Time evolution of the pressure in the simulation shown in Fig. 2. Prior to steady state there is a transient period where fronts develop and the pressure rises. At steady state the pressure fluctuates around a mean value.

value. This is emphasized in the fluctuating pressure with a time invariant average value. Since the physical length of the network $L=6$ mm is small, the pressure drop $\Delta P \sim 300$ Pa is also relatively small.

When the system is started out in a completely different matter, where the phases are totally mixed randomly before the simulation, we see the same behavior in pressure at steady state as shown in Fig. 4. However, the relaxation is much faster, and the transients vanish at an earlier stage. Hence, the system is initially closer to steady state, but the outcomes of the two ways of setting up the system are statistically similar.

Even though we claim that the steady-state fluid configurations are independent of how the system started out, they do adjust to the physical regime to which they are subjects. Changes in the interplay between drainage and imbibition controlled by the capillary number Ca, and in the saturation of the phases, will affect how the fluids organize. In steady-state fluid clusters may break up and smaller clusters merge together, but the statistical distribution of these should, however, stay invariant.

A. Fluid cluster distribution

We study the distribution of clusters of nonwetting fluid. The size of a cluster is denoted as s, and the distribution of cluster sizes is $N(s)$. At a given saturation of nonwetting fluid, a spanning cluster occurs in a way resembling the percolation transition. Near this phase transition, the cluster distribution will be dominated by a singularity, attaining the scaling form

$$N(s) \propto s^{-\tau} f\left(\frac{s}{s^*}\right), \tag{5}$$

where $f(u)$ is a cutoff function that decays faster than any power of u for $u \gg 1$ and is constant for $u \ll 1$. τ is the polydispersity critical exponent. There is also an issue in connection to how we define the clusters. Unlike pure percolation, we here allow bonds in the network to be partly filled; hence a criterion is needed to determine whether or not such a bond contains a connecting part of a cluster. To do this we introduce a clip level and say that two nodes in the network take part in a nonwetting cluster if the level of wetting fluid separating two nonwetting bubbles in the bond is less than the value of the clip level. We justify the clip level by assuming that small bubbles of wetting fluid will become unstable and subsequently coat to the walls of the pore space. The issue of how to classify clusters will also be present in experimental studies. In the following we set the clip level to $\sim 1\%$ of the total volume in the pore space included in the connecting bond.

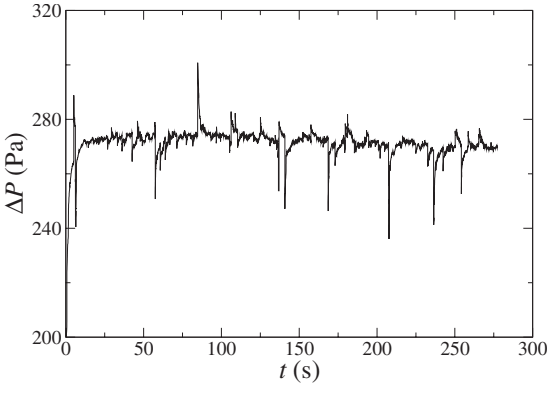

FIG. 4. Pressure as a function of time for a simulation starting with the two phases completely mixed. The relaxation of the pressure is faster than for that of Fig. 3.

According to Eq. (5) there is a characteristic cluster size s^* that controls the cutoff function in the cluster distribution $N(s)$. For a given saturation of the nonwetting fluid S_{nw}, the cluster size distribution of this phase will undergo a transition where s^* diverges—within the limits of finite-size effects—and the cutoff function goes toward a constant. We denote this point as the critical saturation S_c. For low values of S_{nw}, only small disconnected nonwetting clusters will appear, but as S_c is approached from below, larger spanning clusters form. For values of S_{nw} significantly larger than S_c, most of the phase saturation is found within the largest appearing cluster and consequently the cutoff function in Eq. (5) reappears. In Fig. 5, different values of S_{nw} are shown. We see a transition where large clusters form in the system as S_{nw} is increased.

The distribution of nonwetting clusters shown in Fig. 6 yields a value of the polydispersity exponent $\tau = 2.27 \pm 0.08$ for $\mathrm{Ca} \sim 10^{-2}$. This is higher than the value for ordinary three-dimensional percolation, which is $\tau \approx 2.18$ [12]. It is interesting to note that in [13] a value of τ less than the two-dimensional percolation value was reported for a simulation using a regular square lattice. However, there is no reason why one should expect percolation behavior in this system, as the clusters here are highly correlated through the viscous force fields mediated through the tortuous pore space. Also, due to the capillary forces, the nonwetting fluid has a much higher tendency to occupy the volume around the pore bodies than the wetting fluid [14], here represented by the volume around the nodes in the network. In addition, small fractions of wetting fluid can effectively break off large nonwetting clusters and hence alter the situation compared to percolation.

We started out this work by pointing out the similarities between the problem at hand and emulsions. The polydisper-

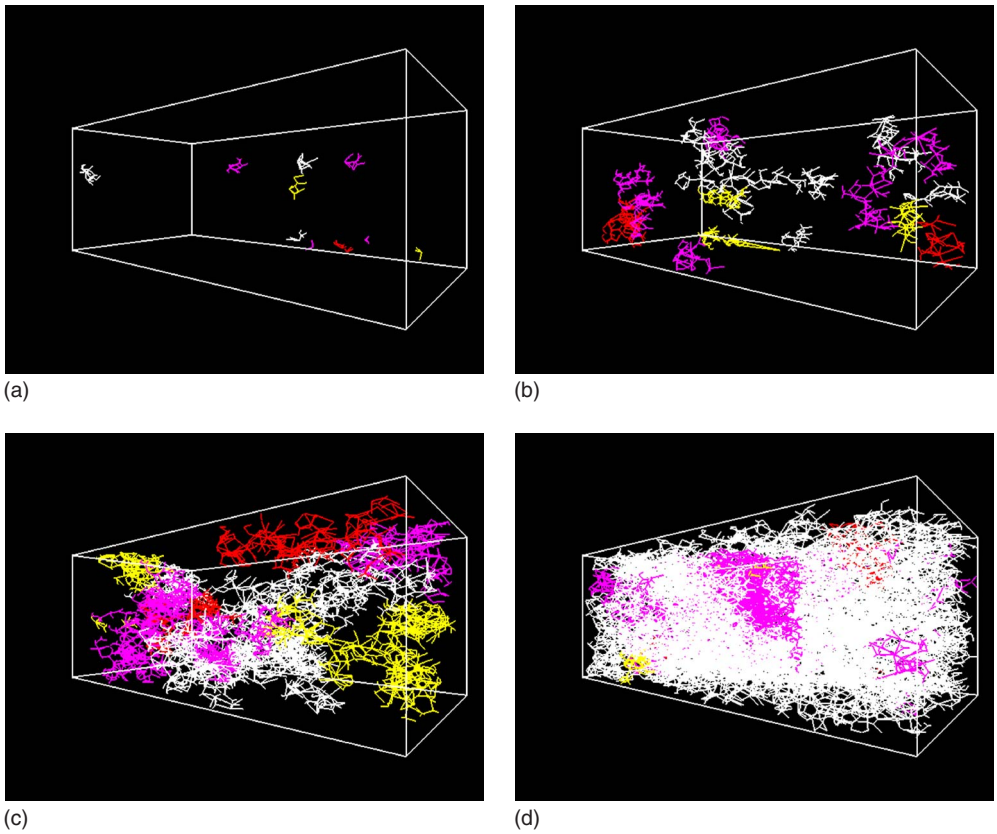

FIG. 5. (Color online) Four configurations of nonwetting clusters at steady state and Ca=1.5×10^{-2}. For illustration only the largest clusters are marked using different colors or grayscales which makes it possible to distinguish them even if they appear close to each other in the model. In (a) $S_{nw}=0.59$ with no large connected nonwetting clusters present. In (b)–(d) nonwetting saturation is $S_{nw}=0.65$, $S_{nw}=0.67$, and $S_{nw}=0.71$. Spanning nonwetting clusters start to form at $S_c\approx0.7$.

sity exponent has been measured, e.g., in micellar solution of sodium dodecyl sulfate, and it has been found to be consistent with the prediction of the dynamical droplet model, which is $\tau=2.21$ [15]. This value is different from the one we report here but quite similar to the ordinary three-dimensional percolation.

The fact that fluid volume is unequally distributed throughout our network with a much larger fraction directly around the nodes will affect values of both S_c and τ. The values of S_c, where we obtain power-law distributions of the cluster sizes, are significantly higher than for similar networks in pure percolation [12], but S_c is a critical point that is highly dependent on the model and flow regimes in which it is encountered. The whereabouts of this point will vary from model to model and different materials and—as will be discussed later in this paper—the nature of the flow.

However, within the framework of the critical processes discussed above, it is believed that the value of τ will be invariant within large classes of topologically different media. Change in the viscosity ratio has been shown in many studies, e.g., Refs. [16–18], to have an impact on transient regimes of drainage. Whether or not this will affect the critical behavior of the cluster size distribution in steady-state processes is an open question. Experimental work has been done on a quasi-two-dimensional bead pack with continuous injection of air and a glycerol/water mixture to study fluid cluster dynamics in steady state [8]. Air cluster dynamics has also been studied experimentally on a similar model, injecting air into a highly viscous defending fluid [19]. In both cases the viscosity ratio $M\simeq10^{-4}$ was far from unity. For high Ca it was seen in both experiments that distinct transients such as viscous fingering became completely disintegrated after some time. This resembles the situation in our simulations even though we use a different viscosity ratio. We therefore believe that the underlying process of going from transients to a steady-state situation is universal for a wide range of viscosity ratios as long as the wetting conditions stay invariant.

B. Critical saturation

For values of $S_{nw}>S_c$ there will be a finite probability $P_\infty>0$ for a fragment of nonwetting fluid to be attached to the largest spanning cluster. In order to calculate P_∞ we identify the largest nonwetting cluster s_{max} and define

$$P_\infty=\frac{s_{max}}{\sum_s sN(s)}. \tag{6}$$

This quantity is the order parameter of our system.

Since our system is finite, we see a gradual increase in P_∞ near S_c, making it harder to pinpoint exactly where the transition takes place. However, it is sharp enough to give clear indications that the transition is indeed second order.

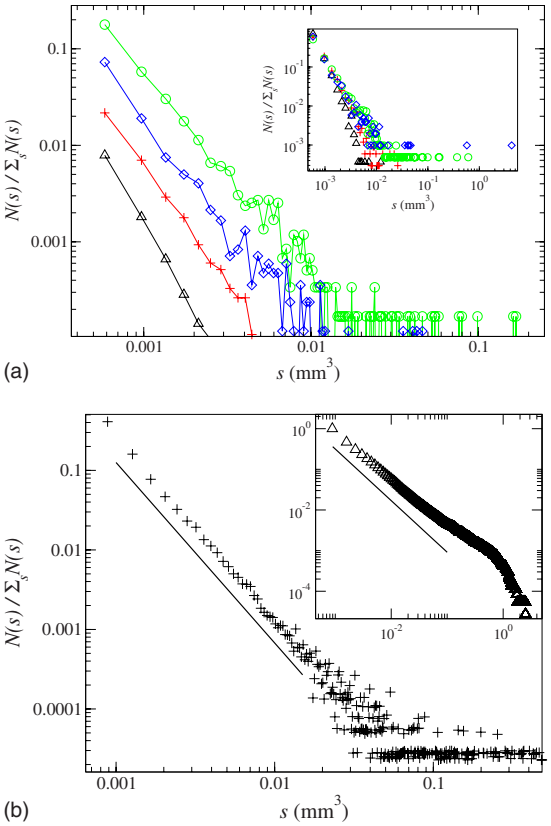

FIG. 6. (Color online) Frequency of nonwetting clusters, where the sets (△), (+), (○), and (◇) are distributions from the realizations in Figs. 5(a)–5(d). The sets are artificially separated for clarity. The actual frequencies are shown in the inset. In the lower figure the nonwetting cluster size distribution for an average over 20 samples with different initial configurations is displayed. The slope, which is a guide for the eyes, indicates a critical exponent $\tau = 2.27 \pm 0.08$ over the range where the power-law behavior applies. In the inset the respective cumulative distribution is displayed with a draw slope of $\tau+1$. The actual descent is not that steep.

Results for P_∞ vs S_{nw} for different Ca are shown in Fig. 7. The spanning clusters of nonwetting fluid occur at saturations well above 50%. This may not be taken as a reflection of the Bancroft rule since this does not imply that the clusters of wetting fluids form spanning clusters at low wetting saturation.

The critical saturation, S_c, is defined as the value of S_{nw} for which P_∞ has the largest derivative with respect to S_{nw}. We find that S_c depends on the capillary number Ca as (inset of Fig. 7)

$$S_c = A + B \log_{10}(\mathrm{Ca}), \tag{7}$$

with $A=0.8$ and $B=0.063$. However, the fluctuations in S_c are extremely small compared to the range of Ca, and below a value $\mathrm{Ca} \sim 10^{-4}$ we do not see much changes in behavior. S_c also flattens toward a constant for high Ca.

In the work by Payatakes and co-workers [4], different regimes of cluster transport under steady-state conditions

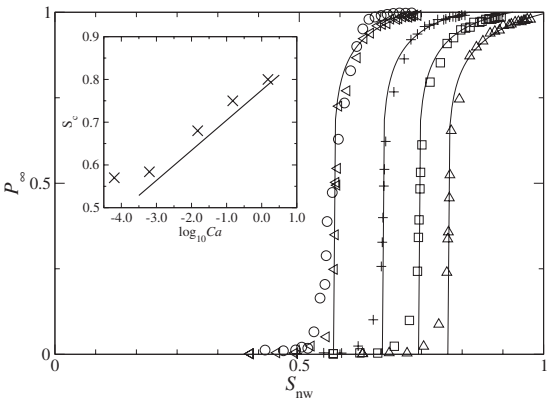

FIG. 7. P_∞, defined in Eq. (6), as a function of S_{nw} for different Ca; (◁) for $\mathrm{Ca}=6.5\times10^{-4}$, (+) for $\mathrm{Ca}=1.5\times10^{-2}$, (□) for $\mathrm{Ca}=1.5\times10^{-1}$, and (△) for $\mathrm{Ca}=1.5$ The inset shows the respective values of S_c, as determined from P_∞ vs S_{nw} plotted against $\log_{10}$ Ca. The last curve (○) for $\mathrm{Ca}=6.5\times10^{-5}$ does not differ significantly in S_c from that of $\mathrm{Ca}=6.5\times10^{-4}$, but it has a slightly less sharp rise.

were proposed and studied. For relatively high Ca, a flow regime denoted by *drop-traffic flow* was proposed, characterized by transport of small disconnected nonwetting blobs. This was due to vigorous fragmentation of larger fluid clusters and resembles well the processes we observe when transient nonwetting fluid patterns disintegrate an approaching steady state. In a way this behavior resembles emulsion. Nevertheless, beyond a certain threshold in S_{nw} spanning nonwetting clusters will form and eventually create connected pathways through the system. Such a process was also discussed in the aforementioned studies. We have argued that this threshold is dependent on Ca and is related to the equilibrium process of continuously dynamic breakup and coalescence of clusters at steady state. In the extreme case of very high Ca, i.e., zero capillary forces, emulsion should be present in the entire range of S_{nw}, hence a critical saturation close to unity.

Recent experimental flooding studies [20] using x-ray microtomography to detect immiscible organic fluids on pore scale indicate that the surface area-to-volume ratio of individual clusters decrease when the saturation decreases. This is consistent with our Fig. 5 where we see a clear cutoff for the large clusters for $S_{nw} < S_c$.

IV. CONCLUSION

In this paper we have aimed to study structure formation of nonwetting fluid clusters during two-phase flow in porous media under steady-state conditions. We observe that the flow configuration indeed forms a state in that it does not depend on how the system is initially prepared. However, the saturations of the phases largely affect the steady-state configurations, and we claim that there is a second-order percolationlike phase transition resembling the phase inversion transition occurring in emulsions. We determine one critical exponent that characterizes this transition and find it to be different from that of the corresponding percolation problem and the exponent measured in amphiphilic systems. In con-

nection to this critical behavior, we have also observed that the critical saturation, S_c, is a function of the capillary number, i.e., the global flow rate Q. This may be of importance when such flow occurs in radial geometries where the flow becomes faster, closer to the core. Our results indicate that the possibility of a phase inversion transition may occur at some radius.

ACKNOWLEDGMENTS

We thank K. J. Måløy, H. G. Rueslåtten, and M. Sahimi for interesting discussions. This work was supported by the Norwegian Research Council (NFR) under Grant No. 154535/432 and the PETROMAKS project "Towards a Digital Core Laboratory" NFR under Grant No. 180296/S30.

[1] O. D. Velev, K. D. Danov, and I. B. Ivanov, J. Dispersion Sci. Technol. **18**, 625 (1997).

[2] M. Sahimi, *Flow and Transport in Porous Media and Fractured Rock* (VCH, Weinheim, 1995).

[3] C. M. Marle, *Multiphase Flow in Porous Media* (Graham and Trotman, London, 1981).

[4] D. G. Avraam, G. B. Kolonis, T. C. Roumeliotis, G. N. Constantinides, and A. C. Payatakes, Transp. Porous Media **16**, 75 (1994); D. G. Avraam and A. C. Payatakes, J. Fluid Mech. **293**, 207 (1995); Ind. Eng. Chem. Res. **38**, 778 (1999).

[5] G. N. Constantinides and A. C. Payatakes, AIChE J. **42**, 369 (1996).

[6] M. Hashemi, M. Sahimi, and B. Dabir, Phys. Rev. Lett. **80**, 3248 (1998).

[7] M. Hashemi, B. Dabir, and M. Sahimi, AIChE J. **45**, 1365 (1999).

[8] K. T. Tallakstad, M.Sc. thesis, University of Oslo, 2007; K. T. Tallakstad, H. A. Knudsen, T. Ramstad, G. Løvoll, K. J. Måløy, R. Toussaint, and E. G. Flekkøy, Phys. Rev. Lett. **102**, 074502 (2009).

[9] H. A. Knudsen, E. Aker, and A. Hansen, Transp. Porous Media **47**, 99 (2002).

[10] P. E. Øren, S. Bakke, and O. J. Arntzen, 1997 SPE Annual Technical Conference and Exhibition, Paper No. SPE38880 (1997); SPEJ **3**, 324 (1998); P. E. Øren and S. Bakke, J. Pet. Sci. Eng. **39**, 177 (2003).

[11] See EPAPS Document No. E-PLEEE8-79-059903 for video of the simulation. For more information on EPAPS, see http://www.aip.org/pubservs/epaps.html.

[12] D. Stauffer and A. Aharony, *Introduction to Percolation Theory* (Taylor & Francis, London, 1994).

[13] T. Ramstad and A. Hansen, Phys. Rev. E **73**, 026306 (2006).

[14] L. Yu and N. C. Wardlaw, J. Colloid Interface Sci. **109**, 461 (1986); **109**, 473 (1986).

[15] E. Ducros, S. Haouache, J. Rouch, K. Hamano, K. Fukuhara, and P. Tartaglia, Phys. Rev. E **50**, 1291 (1994); T. Isojima, S. Fujii, K. Kubota, and K. Hamano, J. Chem. Phys. **111**, 9839 (1999).

[16] R. Lenormand, E. Touboul, and C. Zarcone, J. Fluid Mech. **189**, 165 (1988).

[17] R. Lenormand and C. Zarcone, Phys. Rev. Lett. **54**, 2226 (1985).

[18] G. Løvoll, Y. Meheust, R. Toussaint, J. Schmittbuhl, and K. J. Måløy, Phys. Rev. E **70**, 026301 (2004).

[19] A. Vedvik, G. Wagner, U. Oxaal, J. Feder, P. Meakin, and T. Jøssang, Phys. Rev. Lett. **80**, 3065 (1998).

[20] G. Schnaar and M. L. Brusseau, Environ. Sci. Technol. **40**, 6622 (2006).